ABSTRACT

AN ANALYSIS OF CHANGES IN THE MAGNETIC FIELD OF ACTIVE REGION 9415 AFTER THE 2001 APRIL 6 SOLAR FLARE

by
Juli Marya Stoltz

The objective of this study was to further the current understanding of the correlation between solar flares and magnetic flux change. The average gradient of the magnetic flux around the neutral line of Active Region 9415 and the locations of the magnetic flux centers-of-mass in both polarities in AR 9415 were determined. Subsequent to the 2001 April 6 flare, there was a statistically significant mean increase of 0.00208 G/km in the average gradient. Prior to the flare, the magnetic flux centers-of-mass became increasingly sheared along the neutral line. After the flare, this shear suddenly decreased and the magnetic flux centers-of-mass converged towards the neutral line.

Presently, solar flares are believed to result when an active region relaxes towards the potential field configuration, i.e., the minimum energy state. Hence, magnetic shear, a measure of non-potentiality, is expected to decrease after a flare. If in fact magnetic gradient is proportional to magnetic shear, the increase in the average gradient implies that the magnetic shear around the neutral line increased following the flare. However, the sudden decrease in the magnetic flux center-of-mass separation parallel to the neutral line indicates an overall decrease in the magnetic shear of the whole active region. Therefore, it can be concluded that the magnetic shear kept increasing in local areas in spite of an overall decrease on the large scale subsequent to the flare. The local increase of magnetic shear in the neutral line region is believed to be associated with the convergence of magnetic fluxes in both polarities towards the neutral line.

AN ANALYSIS OF CHANGES IN THE MAGNETIC FIELD OF ACTIVE REGION 9415 AFTER THE 2001 APRIL 6 SOLAR FLARE

by
Juli Marya Stoltz

A Thesis
Submitted to the Faculty of
New Jersey Institute of Technology
in Partial Fulfillment of the Requirements for the Degree of
Master of Science in Applied Physics

Federated Physics Department

August 2005

APPROVAL PAGE

AN ANALYSIS OF CHANGES IN THE MAGNETIC FIELD OF ACTIVE REGION 9415 AFTER THE 2001 APRIL 6 SOLAR FLARE

Juli Marya Stoltz

Dr. Haimin Wang, Thesis Advisor — Date
Distinguished Professor of Physics, NJIT

Dr. Dale E. Gary, Committee Member — Date
Professor of Physics, NJIT

Dr. Jeongwoo Lee, Committee Member — Date
Associate Research Professor of Physics, NJIT

BIOGRAPHICAL SKETCH

Author: Juli Marya Stoltz

Degree: Master of Science

Date: August 2005

Undergraduate and Graduate Education:

- Master of Science in Applied Physics
  New Jersey Institute of Technology, Newark, NJ, 2005

- Bachelor of Science in Physics,
  Montclair State University, Upper Montclair, NJ, 2004

- Bachelor of Science in Mathematics,
  Montclair State University, Upper Montclair, NJ, 2004

Major: Applied Physics

To my grandfather, Edmund Stolarz, in thanks for all the astronomy articles

ACKNOWLEDGMENT

I would like to express my deepest appreciation to Dr. Haimin Wang for not only serving as my thesis advisor, but also providing superb direction and always making time to answer my questions.

I would like to offer special thanks to Dr. Dale E. Gary and Dr. Jeongwoo Lee for serving on my committee. I would also like to thank Dr. Gary and Dr. Lee for their thesis advice.

In addition, I would like to extend my sincere thanks to Yan Xu for serving as my IDL advisor and allowing me to share his workspace.

I would also like to thank the Stanford-Lockheed Institute for Space Research for the use of their MDI magnetograms.

Finally, I would like to express my appreciation to my fellow graduate students in the Physics Department for their support. In particular, I would like to thank Preethi Ganapathy, Angelo Verdoni, and, especially, Sam Tun for their invaluable help with IDL.

TABLE OF CONTENTS

TABLE OF CONTENTS
(Continued)

Chapter **Page**

LIST OF FIGURES

LIST OF FIGURES
(Continued)

CHAPTER 1

BACKGROUND

1.1 Objective

The objective of this project is to further the current understanding of the correlation between solar flares and magnetic flux change. The average gradient of the magnetic flux along the neutral line of Active Region 9415 is examined before and after the 2001 April 6 solar flare. The purpose is to determine whether or not the solar flare produced a permanent change in the average gradient in this region. In addition, the separation between the positive magnetic flux center-of-mass and the negative magnetic flux center-of-mass of Active Region 9415 is determined at points before and after the flare. The purpose is to examine the relative motion between these centers-of-mass around the time of the flare.

1.2 Definition of Solar Flare

A solar flare is an explosive release of energy that results from magnetic field line reconnection on the Sun. The energy released during a solar flare is mainly in the form of electromagnetic radiation. Energetic solar flares release energies in the order of 10^{32} erg in 10^4 s while small flares release energies less than or equal to 10^{30} erg in approximately 10^3 s. There is, however, no lower limit to possible flare energies (Schrijver 2000).

The two major classifications of solar flares are confined and eruptive. In a confined flare, magnetic field lines merge without overlying field lines being opened. In an eruptive flare, overlying field lines are blown open (extended out into space) and

subsequently reconnect. Magnetic field lines may open as a result of newly emerging magnetic flux, field line shear exceeding a critical limit, or some form of wave disturbance (Svestka 2003).

The phases of a large solar flare include: the precursor phase, the impulsive or the flash phase, and the main phase. The precursor phase includes phenomena that precede the main flare event such as filament activation, filament eruption, surges, and the onset of a coronal mass ejection (CME). The impulsive phase is characterized by the sudden release of energy. During this phase, the radiation is largely nonthermal. A collection of emission spikes is observed in the radio, microwave, extreme-ultraviolet, X-ray, and gamma-ray spectrum. However, the bulk of the emission is radiated during the main phase, which is characterized by radiation that is largely thermal (Schrijver 2000).

1.3 Definition of an X-Class Solar Flare

Solar flares are classified according to their X-ray brightness in the 1 to 8 angstrom wavelength range. B-class solar flares have peak intensities less than 10^{-6} W/m^2 in this wavelength range. C-class solar flares have peak intensities greater than or equal to 10^{-6} W/m^2 and less than 10^{-5} W/m^2. M-class solar flares have peak intensities greater than or equal to 10^{-5} W/m^2 and less than 10^{-4} W/m^2. X-class solar flares have peak intensities greater than or equal to 10^{-4} W/m^2. Therefore, a solar flare classified as an X5.6 has a peak intensity of 5.6×10^{-4} W/m^2 in the 1 to 8 angstrom wavelength range.

While B- and C-class solar flares produce few, if any, noticeable consequences on Earth, X-class flares can cause planet-wide radio blackouts and long-lasting radiation storms (Phillips 2005).

1.4 Definition of Magnetograph

1.4.1 Magnetograms

A magnetograph is an instrument that produces magnetograms by measuring Zeeman splitting. Zeeman splitting is the broadening or splitting of a spectral line into several polarized components when a source is in the presence of a strong magnetic field. The degree of splitting and polarization depend upon the strength of the magnetic field. Zeeman splitting can be measured by taking two narrowband images in a spectral line sensitive to magnetic field. The two measurements are taken with opposite senses of polarization.

A magnetogram is a chart that displays the strength, the polarity, and the distribution of magnetic fields across the disk of the Sun. On a magnetogram, the gray areas indicate no line-of-sight magnetic field, the white areas indicate regions of positive polarity, and the black areas indicate regions of negative polarity (Darling 2005).

1.4.2 The Michelson Doppler Imager

The Michelson Doppler Imager (MDI) is an instrument located on board the Solar and Heliospheric Observatory (SOHO) satellite. MDI is a project of the Stanford-Lockheed Institute for Space Research and is a joint effort of the Solar Oscillations Investigation (SOI) in the W. W. Hansen Experimental Physics Laboratory of Stanford University and the Solar and Astrophysics Laboratory of the Lockheed-Martin Advanced Technology Center. SOHO is a joint European Space Agency (ESA) and National Aeronautics and Space Administration (NASA) mission. SOHO was launched on December 2, 1995 and placed in an elliptical orbit around the first Lagrangian point (L1) (Stanford-Lockheed 2000).

The MDI instrument includes a 1024 x 1024 pixel CCD camera. It measures the line intensities at five positions along the Ni I 6768 angstrom spectral profile alternating between left and right circular polarization modes. At the central positions of four bandpasses, the spectrum line intensities F_1, F_2, F_3, and F_4 are obtained. With these intensities, the line shift parameter is calculated using one of the following equations:

$$\alpha_{l,r} = (F_1 + F_2 - F_3 - F_4)/(F_1 - F_3)$$

when the numerator is positive and

$$\alpha_{l,r} = (F_1 + F_2 - F_3 - F_4)/(F_4 - F_2)$$

when the numerator is negative. Then, the line shift parameter is converted to the velocity using an empirical lookup table. Finally, the magnetic field strength is determined by calculating the difference between the velocities derived at left and right circular modes using the following equation:

$$B_m = (V_l - V_r)/2.84$$

The preceding calculations are all performed onboard SOHO and only secondary observables, such as magnetograms, are sent back to Earth (Qiu 2003).

CHAPTER 2

SOLAR FLARES AND CHANGES IN MAGNETIC FLUX

2.1 Solar Flare Models

2.1.1 Magnetic Breakout Model

In the magnetic breakout model, a multipolar topology consisting of a sheared arcade and neighboring flux systems initially exists. Reconnection between the sheared arcade, which lies near the neutral line, and the neighboring flux systems removes unsheared field from above the sheared arcade. This reconnection allows the sheared arcade to open producing a flare, filament eruption, and CME (Antiochos 1998). See Figure 2.1.

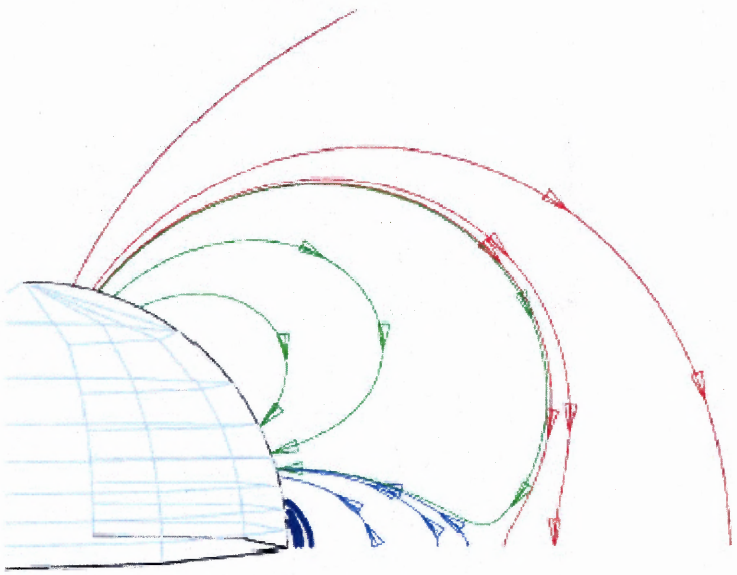

Figure 2.1 Illustration of the potential magnetic field in the magnetic breakout model. The different colors indicate the different flux systems.
Source: Antiochos, DeVore, & Klimchuk 1999

Deng et al. (2005) claim that this model can explain the distinctive features of the 2000 June 6 flare in NOAA Active Region 9026, which include flare-related penumbral decay, central umbral darkening, associated CME, and associated filament eruption. The

flare related penumbral decay is believed to be the result of a change in the orientation of the magnetic field lines to a more vertical configuration. According to Deng et al., the magnetic breakout model suggests that the magnetic flux in the central umbrae will increase as magnetic field lines move away from the peripheral penumbrae as a result of an increase in inclination angle. The fact that only a small flux increase was actually seen is thought to be due to Zeeman saturation.

2.1.2 Emerging Flux Model

The emerging flux model consists of three phases. During the preflare phase, new magnetic flux emerges beneath the flare filament. This results in the heating of the current sheet between the old and the new magnetic flux. The impulsive phase begins when the current sheet loses equilibrium at a critical height. During the impulsive phase, the current sheet expands rapidly. The main phase begins when the current sheet reaches a new steady state with marginal reconnection (Priest & Heyvaerts 1974). See Figure 2.2.

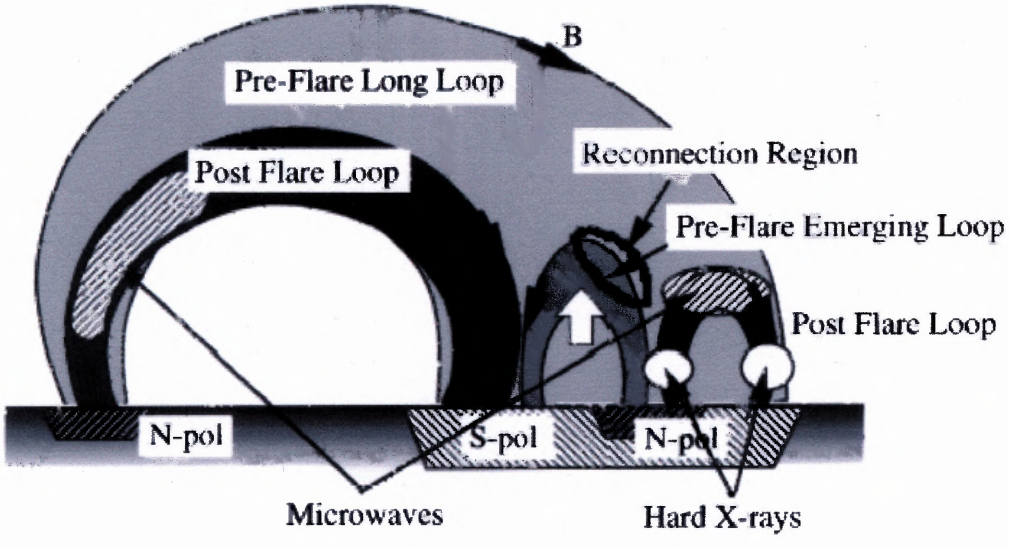

Figure 2.2 Illustration of the emerging flux model.
Source: Nishio et al. 1997

2.1.3 Simple 2-D Quadrupolar Magnetic Reconnection Model by Liu et al. (2005)

According to the simple 2-D quadrupolar magnetic reconnection model proposed by Liu et al. (2005), two separate magnetic flux systems are joined at a δ sunspot, where umbrae of opposite polarities lie within a common penumbra. During the flare, two new sets of loops, a compact loop and a large-scale loop, are created as a result of magnetic reconnection between the converging magnetic flux systems. See Figure 2.3.

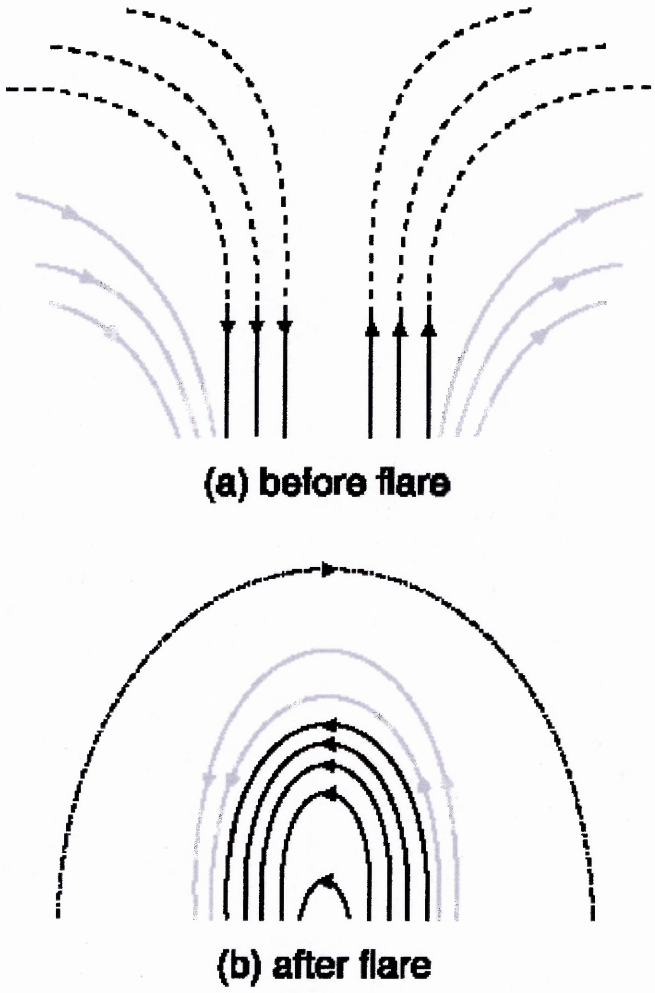

Figure 2.3 Illustration of the simple 2-D quadrupolar magnetic reconnection model by Liu et al. (2005). (a) Preflare magnetic field configuration. Penumbral fields are in gray and umbral fields are in black. (b) Postflare magnetic field configuration. The dash-dotted line represents the connection between two points far apart.
Source: Liu et al. 2005

2.2 Magnetic Shear

Magnetic shear is defined as the product of transverse magnetic field strength and shear angle, which is the angular separation between the directions of the transverse fields and the extrapolated potential fields. Shear is widely regarded as an indicator of nonpotentiality, i.e., departure from the minimum energy state. According to several solar flare models (e.g., Amari et al. 2000), photospheric shear motion builds up free magnetic energy by forming non-potential magnetic field configurations. It is believed that a flare results when the shear exceeds a threshold value and the magnetic field is restored to a more potential configuration.

2.3 Transient Versus Permanent Changes in Magnetic Field

The magnetic field changes that have been observed in association with some solar flare events can be classified as either transient or permanent. A transient change occurs only during a flare. The magnetic field returns to the preflare state following the flare event. A permanent change is a change in the magnetic field between the preflare state and the postflare state that is irreversible (Qiu & Gary 2003).

Although this study is concerned with permanent rather than transient changes in the solar magnetic field, it is important to note that the magnetic field measurements made during a flare are believed to be distorted. Qiu & Gary (2003) examined an apparent transient sign reversal that occurred in small areas of the MDI magnetograms from the impulsive phase of the 2001 April 6 flare in AR 9415. They refer to this magnetic transient as a magnetic anomaly. In order to ascertain the source of the magnetic anomaly, Qiu & Gary simulated MDI magnetic field measurements for a line

profile that deviates from the standard quiescent profile. According to their study, it is likely that the magnetic anomaly was caused by a distortion in the MDI measurements when the Ni I 6768 angstrom line was temporarily turned from absorption into emission or was broadened significantly with a strong central reversal as a result of a nonthermal beam impact on the umbral atmosphere.

As for permanent changes observed in association with solar flares, the findings of previous studies are widely varied. Kosovichev & Zharkova (2001) found a permanent decrease in magnetic flux in addition to a short-term magnetic transient for the 2001 July 14 solar flare. However, Chen et al. (1994) studied over 20 M-class flares and found no apparent flare-related change in the magnetic fields. Spirock, Yurchyshyn, &Wang (2002) studied the 2001 April 2 X20 flare and found a 6 x 10^{20} Mx increase in the magnetic flux of the leading polarity, but no change in the magnetic flux of the following polarity. Wang et al. (2002) studied 6 X-class flares. They found a permanent increase in the magnetic flux of the leading polarity and some decrease in the magnetic flux of the following polarity for all of the flare events.

2.4 Gradient of Line-of-Sight Magnetic Field

It has been observed that active regions with neutral lines across which the gradient of the line-of-sight magnetic field is large tend to have strongly sheared core field along the neutral line (Zirin & Liggett 1987). This observation has lead scientists to explore the possibility of using the gradient of line-of-sight magnetic field to predict CMEs and solar flares. If sufficiently developed, these methods could improve the forecasting of possibly

damaging space weather and improve the current understanding of CMEs and solar flares because line-of-sight field is more easily measured and analyzed than full vector fields.

Falconer, Moore & Gary (2002) measured the length of strong shear (L_{SS}) for 12 bipolar active regions using 17 magnetograms. L_{SS} is the length of the portion of the main neutral line on which the observed transverse field is greater than 150 G and has a shear angle greater than 45°. Falconer, Moore, & Gary concluded that L_{SS} is a measure of the overall nonpotentiality of an active region and significantly correlated with CME productivity.

Subsequently, Falconer, Moore & Gary (2003) measured the strong gradient length (L_{SG}) for the same 12 bipolar active regions in order to determine whether or not it is a viable proxy for L_{SS}. L_{SG} is the length of the portion of the main neutral line on which the potential transverse field is greater than 150 G and the gradient of the line-of-sight field is above some threshold value. Unlike L_{SS}, L_{SG} can be measured from a line-of-sight magnetogram. For the data examined, the threshold value for the gradient of the line-of-sight magnetic field was determined to be in the vicinity of 50 G/Mm. Falconer, Moore, & Gary concluded that L_{SG} is statistically significantly correlated with L_{SS} and CME productivity. Therefore, it is a measure of nonpotentiality.

Wang et al. (2005) propose that magnetic gradient derived from line-of-sight magnetic fields could be used to predict where a major flare may occur. For each of five well-known active regions that produced flares classified as X5 or larger, Wang et al. created three images: a magnetic gradient map, a shear map, and a mask map representing the location of the magnetic neutral lines. The magnetic gradient maps were constructed using line-of-sight magnetograms. The magnetic shear map was constructed

by calculating the product of the observed transverse field strength and the shear angle. Then, the gradient image and the mask image were multiplied in order to create an image of the gradient in the neutral lines only. The shear image and the mask image were multiplied in order to create an image of the shear in the neutral lines only. Finally, a scatter plot of the magnetic shear versus the magnetic gradient was created. The plots of magnetic shear versus magnetic gradient constructed by Wang et al. show a strong positive correlation between magnetic gradient and magnetic shear.

CHAPTER 3

OVERVIEW OF THE SOLAR FLARE OF 2001 APRIL 6

3.1 Overview of the Solar Flare

On 2001 April 6, one of the largest flare events in solar cycle 23 took place. The flare occurred in Active Region 9415, which was located at S20 degrees and E31 degrees. See Figure 3.1. It was associated with a Halo CME (visible around the entire occulting disk), but not a filament eruption. This flare has been classified as an X5.6 flare.

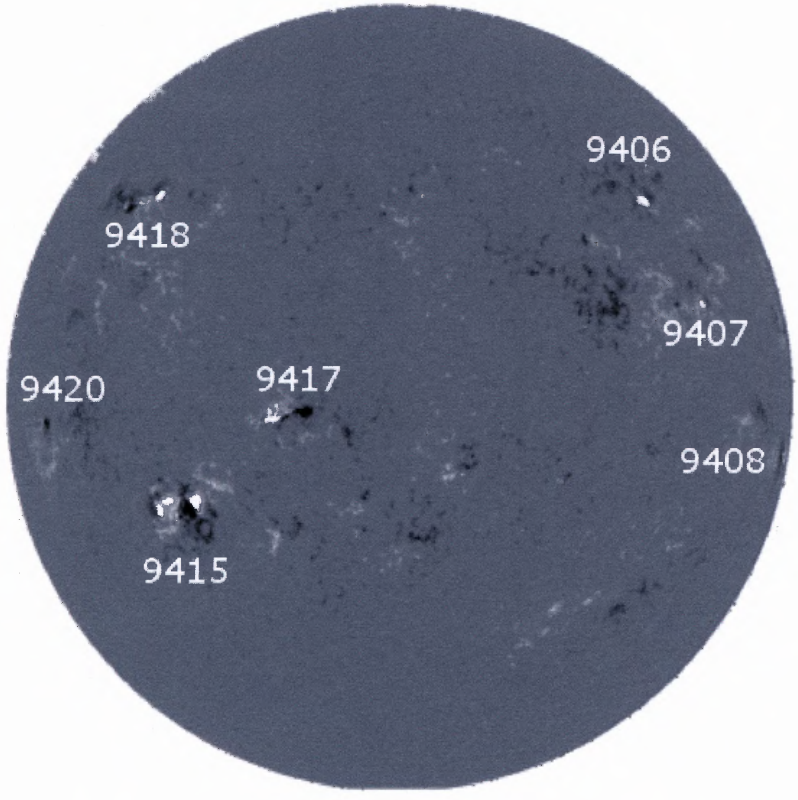

Figure 3.1 Solar disk at 17:00:02 UT on 2001 April 6. The labels are the active region numbers.

Qiu, Lee, & Gary (2004) examined the hard X-ray and microwave emission during the 2001 April 6 flare event and found that this emission can be divided into two distinct phases. The impulsive phase, 19:16-19:23 UT, is characterized by hard X-ray and microwave emissions consisting of several impulsive bursts. Each burst arose sharply, decayed fast, and lasted tens of seconds. The gradual phase, 19:28 UT onward, is characterized by gradual smooth emission at hard X-ray and microwave wavelengths. This single, gradual component lasted for approximately ten minutes.

Qui, Lee, & Gary (2004) found that the gradual component of the flare involved a different emission source than the impulsive component of the flare. In general, emission during the impulsive phase emerged from sources located at the ends of a soft X-ray loop structure. The two sources represent conjugate footpoints of the flare loop structure where electrons precipitated to the chromosphere to produce thick-target hard X-ray emission. From 19:14 to 19:18 UT, the two footpoints approached each other with an average speed of 28 km/s. During the gradual phase, the emission source located in the negative field is close to the emission source from the impulsive phase located in the negative field while the emission source located in the positive field is clearly distinct from the second emission source from the impulsive phase. Hard X-ray and microwave emissions outline the configuration of a flare loop connecting the gradual phase emission sources. During the gradual phase, the emission sources moved away from each other and the neutral line. From 19:30 to 19:40 UT, the footpoints separated with an average speed of 13 km/s. The observed motions of the emission sources reflect continuous magnetic reconnection.

3.2 Changes in the Magnetic Flux

For the X5.6 flare on 2001 April 6 in AR 9415, Wang et al. (2002) found that the magnitude of the following (positive) magnetic flux decreased by 4 x 10^{20} Mx while the magnitude of the leading (negative) flux increased by 4 x 10^{20} Mx. The explanation given for these findings is that more flux became detectable rather than the flux actually increasing.

Wang et al. (2005) plotted the magnetic shear derived from vector magnetograms versus the magnetic gradient derived from line-of-sight magnetograms for the X5.6 flare on 2001 April 6 in AR 9415. See Figure 3.2. The plot revealed a close correlation between these two parameters. Wang et al. produced similar results for four other active regions that produced flares classified as X5 or larger.

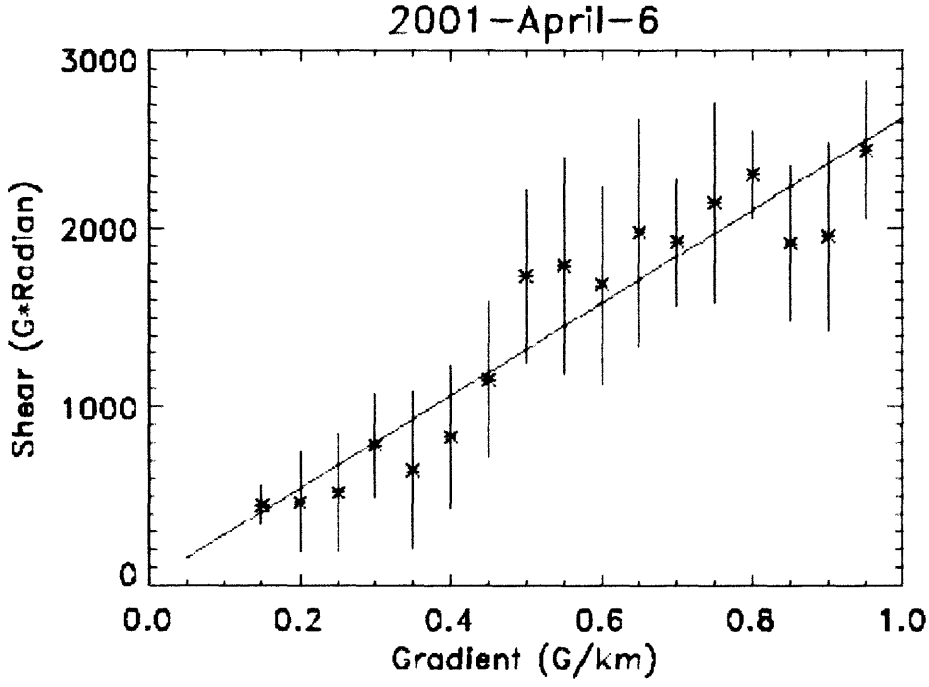

Figure 3.2 Plot of averaged magnetic gradient versus magnetic shear in all the neutral lines identified for the active region 9415 on 2001 April 6.
Source: Wang et al. 2005

CHAPTER 4

DATA ACQUISITION AND REDUCTION

4.1 Data Acquisition

The magnetograms used in this project are MDI magnetograms obtained from the Stanford-Lockheed Institute for Space Research via the Web site http://soi.stanford.edu/production/time_range.html/. The magnetograms span the five hour period from 17:00:02 UT to 21:59:02 UT on 2001 April 6. Magnetogram 24 in the set of 297 magnetograms actually sent was blank. Therefore, it was discarded.

4.2 Data Reduction

All of the data reduction for this project was done in IDL (Interactive Data Language). The data reduction for this project can be divided into the three main parts described below.

4.2.1 Gradient

Prior to taking the gradient of the magnetograms, it was necessary to align, crop, and smooth the magnetograms. The DROT_MAP function in IDL was used to shift the magnetograms so they would all align with the first magnetogram in the set. Then, the portion of the magnetograms corresponding to the region x = 182 to 282 and y = 314 to 414 on the first magnetogram in the set was cropped. See Figure 4.1. Next, the magnetograms were smoothed using the SMOOTH function in IDL. This averaged each pixel value with the values of the pixels in a 5-by-5 square neighborhood.

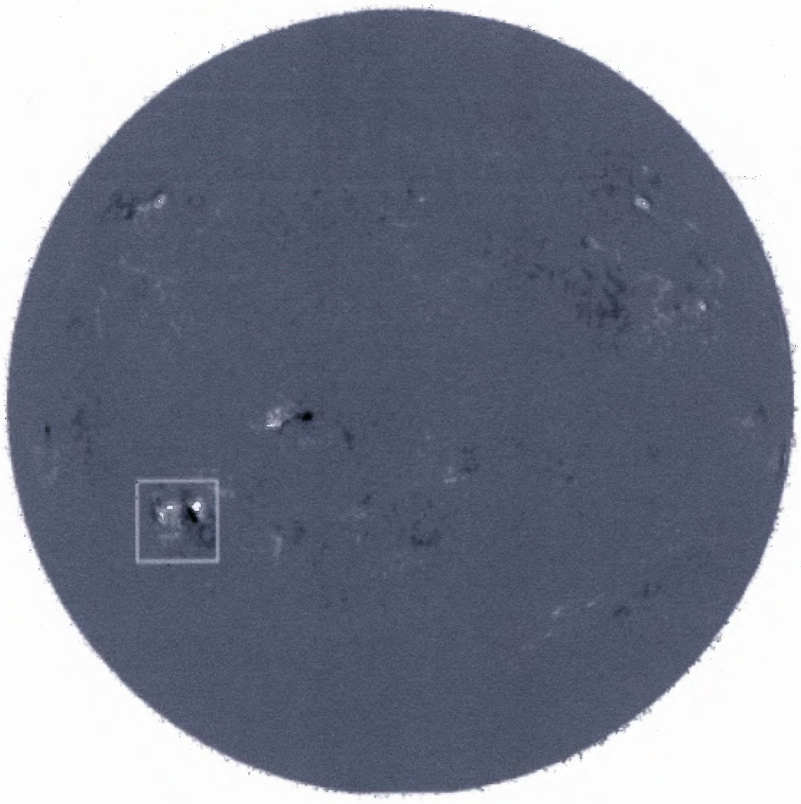

Figure 4.1 Region of the original magnetograms cropped.

The gradient of the magnetograms was taken using a function developed by Dr. R. Molowny-Horas. The magnitude of the gradient of the line-of-sight component of the magnetic field is defined as follows:

$$|\nabla B_z| = \sqrt{(\frac{\partial B_z}{\partial x})^2 + (\frac{\partial B_z}{\partial y})^2}$$

After taking the gradient of the aligned, cropped, smoothed magnetograms, the magnetograms and the gradient images were rotated 36.5° so that the neutral line would appear vertical. In order to obtain this angle of rotation, it was necessary to note that the magnetic flux density should be zero at the neutral line. Therefore, if the neutral line is perfectly straight, a plot of the magnetic flux density versus the column number for any row that the neutral line spans should cross the line $B_z = 0$ at the same point. The proper

angle of rotation was determined through trial and error by rotating the magnetograms by a given angle and then plotting the magnetic flux density versus the column number for the rows that the neutral line spans. Since an angle of 36.5° produced the narrowest magnetic flux density versus column number plot, it was chosen as the proper angle of rotation.

At this point, a magnetogram movie and a gradient movie were made out of the magnetograms and the gradient images.

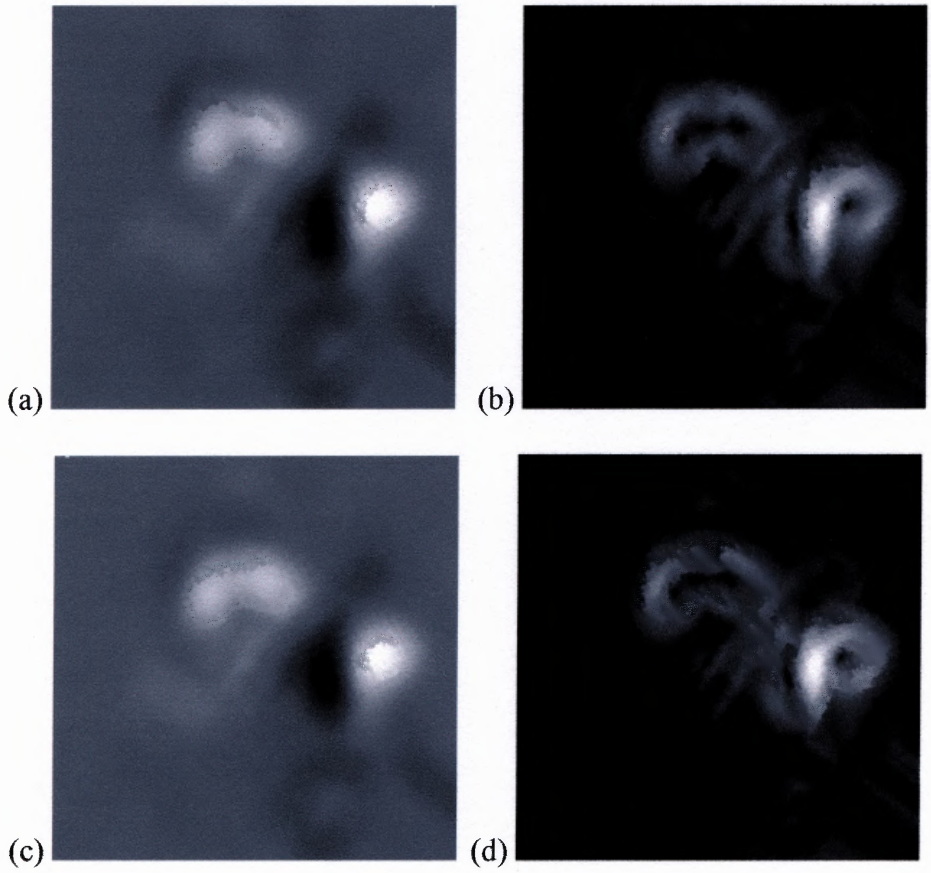

Figure 4.2 (a) Altered version of the MDI magnetogram from 17:00:02 UT. (b) Gradient image of the MDI magnetogram from 17:00:02 UT. (c) Altered version of the MDI magnetogram from 21:59:02 UT. (d) Gradient image of the MDI magnetogram from 21:59:02 UT.

4.2.2 Average Gradient Intensity in the Neutral Line Region

In order to find the average gradient intensity in the neutral line region, it was first necessary to ascertain the minimum size of a box that is able to contain the entire neutral line. See Figure 4.3. By visual inspection, the rows that this box spans were determined to be 35 through 60 on the altered magnetograms. Note that each pixel corresponds to 2''. Since it was difficult to determine the exact path of the neutral line by visual inspection, the columns that the box spans were determined by plotting the magnetic flux density versus the column number for each of rows 35 through 60 for the first and the last magnetograms in the set. Given that the magnetic flux density is expected to be zero at the neutral line, it was possible to determine the columns that the box spans by examining the range of column numbers over which the plots pass through $B_z = 0$. See Figure 4.4. The columns that the box spans were determined to be 72 through 76.

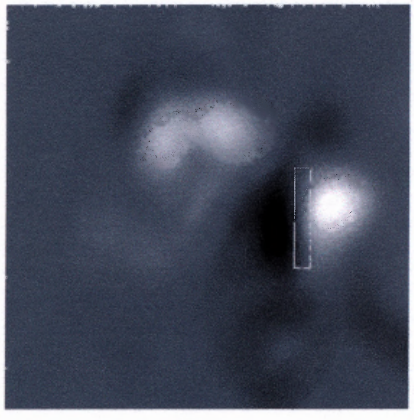

Figure 4.3 Neutral line region.

Once the coordinates of the minimum box were established, the AVG function in IDL was used to find the average gradient intensity in the minimum neutral line region for each gradient image. Since the average gradient intensity was in gauss/pixel, it was necessary to divide by 1424 km/pixel in order to convert the average gradient intensity

into gauss/km. After this was done, the averages were plotted versus the times obtained from the headers of the original magnetograms. Radio flux data for a frequency of 7 GHz from 2001 April 6 were plotted over this plot. These Owens Valley Solar Array (OVSA) data were obtained from Dr. Dale Gary especially for this purpose. The spike in the over plots indicates the time of the flare. See Figure 4.5.

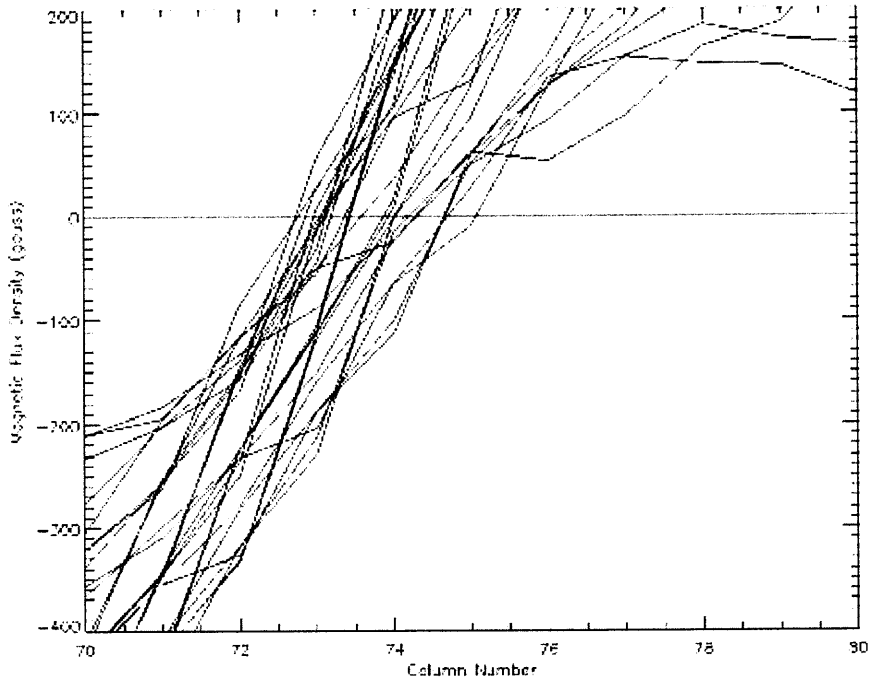

(a)

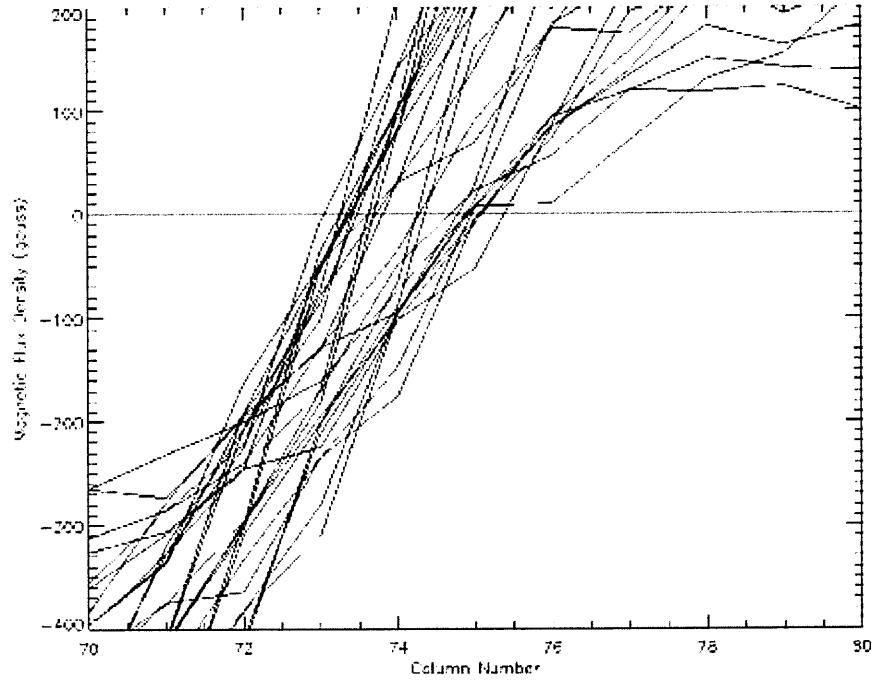

(b)

Figure 4.4 Plot of magnetic flux density versus column number for (a) the 17:00:02 UT magnetogram and (b) the 21:59:02 UT magnetogram.

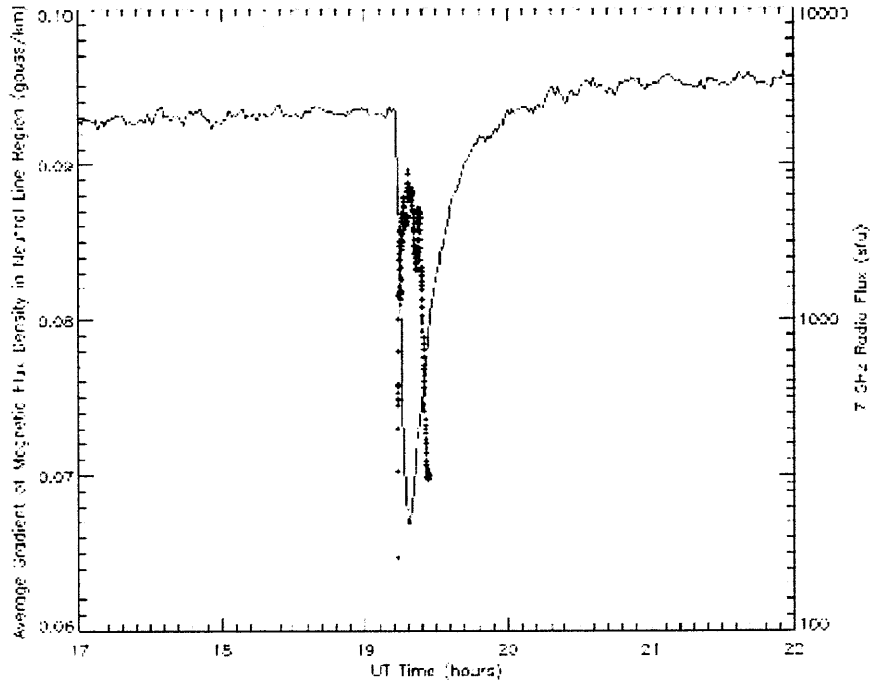

(a)

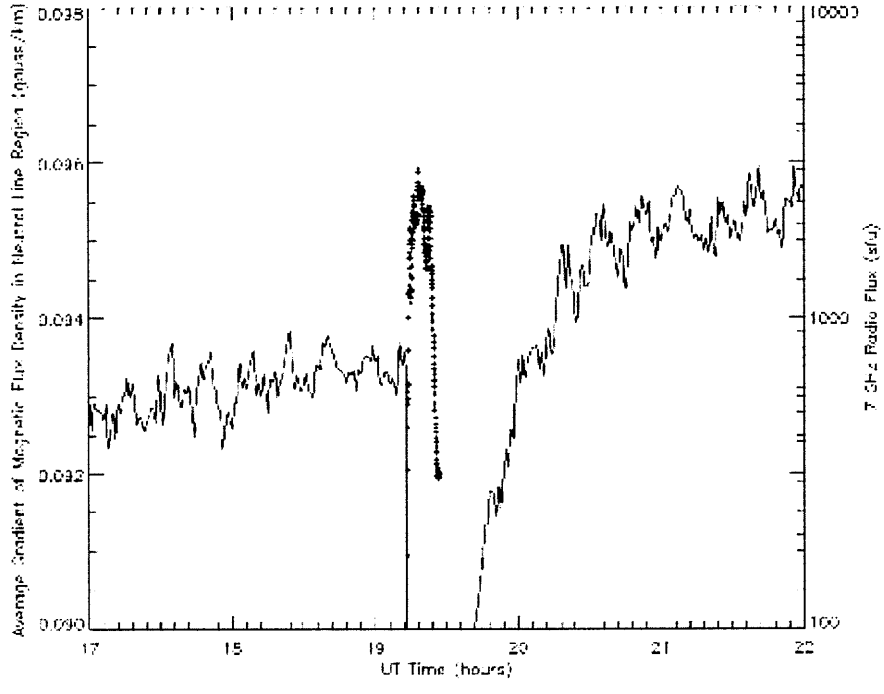

(b)

Figure 4.5 Plot of average gradient intensity in the neutral line region versus time with a range of (a) 0.06 to 0.10 G/km and (b) 0.090 to 0.098 G/km. The solid line indicates the average gradient intensity. The crosses indicate the 7 GHz radio flux.

4.2.3 Magnetic Flux Center-of-Mass Separation

The X- and Y-components of the magnetic flux center-of-mass separation were determined in order to quantitatively study the average motion of magnetic fluxes of opposite polarities. The X-direction refers to the direction perpendicular to the neutral line and the Y-direction refers to the direction parallel to the neutral line. This was done using the center-of-mass method applied by Wang et al. (2005):

$$X_c = \frac{\sum X_i F_i}{\sum F_i};\ Y_c = \frac{\sum Y_i F_i}{\sum F_i}$$

where X_c and Y_c are the center-of-mass positions of magnetic fluxes, F_i is the measured magnetic flux in each pixel, and X_i and Y_i are the positions of the individual pixels.

First, the region X = 59 to 94 and Y = 32 to 64 was selected by visual inspection to encompass the area in which the flare occurred. See Figure 4.6. Then, X_c and Y_c were calculated for positive fluxes by setting the negative fluxes equal to zero and separately for negative fluxes by setting the positive fluxes equal to zero. Next, the differences between the positive and negative center-of-mass positions were calculated by subtracting the negative center-of-mass positions from the positive center-of-mass positions. At this point, the X- and Y-components of the center-of-mass separation were in pixels so it was necessary to multiply by 1424 km/pixel in order to convert to kilometers. Finally, three plots were constructed. The Y-component of the center-of-mass separation versus the X-component of the center-of-mass separation was plotted. See Figure 4.7. In addition, the X-component of the center-of-mass separation and the Y-component of the center-of-mass separation were individually plotted versus time. Radio flux data for a frequency of 7 GHz from 2001 April 6 were plotted over both of these plots. The spike in the over plots indicates the time of the flare. See Figure 4.8.

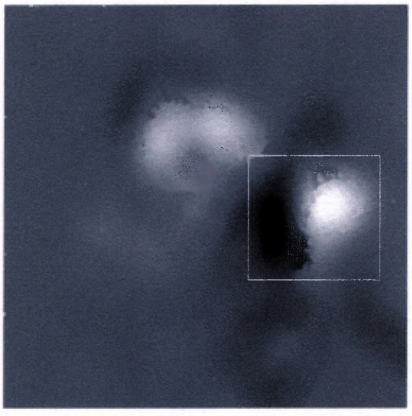

Figure 4.6 Region of magnetic flux center-of-mass analysis.

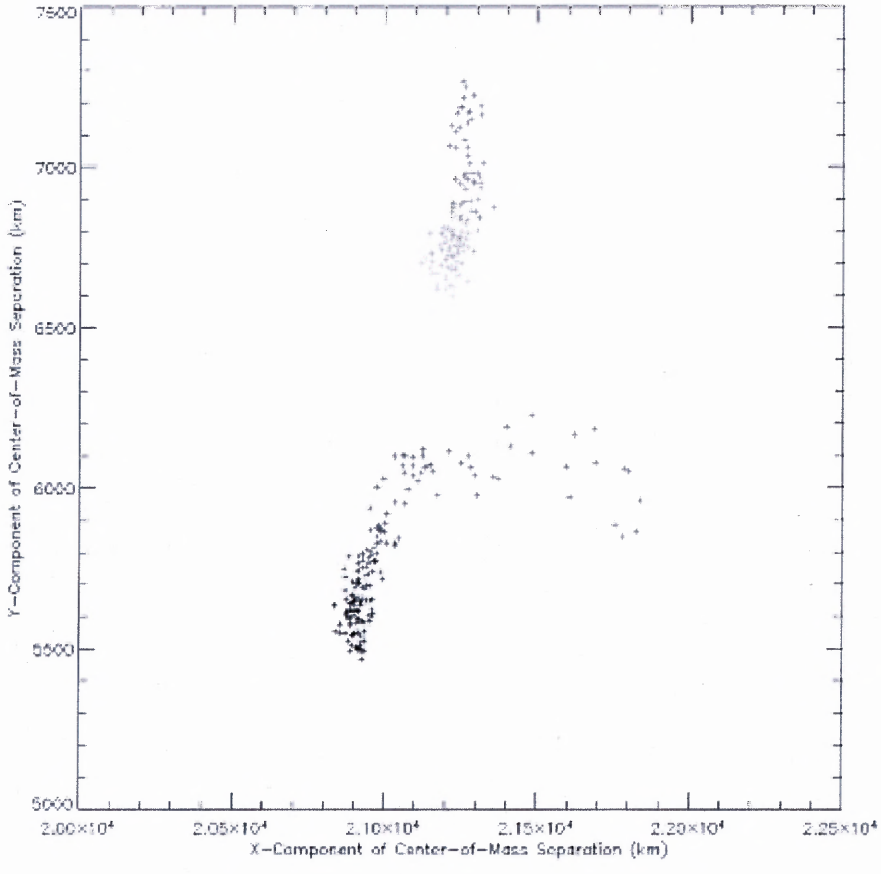

Figure 4.7 Plot of the Y-component of the magnetic flux center-of-mass separation versus the X-component of the magnetic flux center-of-mass separation. The darkening of the color indicates the passage of time in the positive direction.

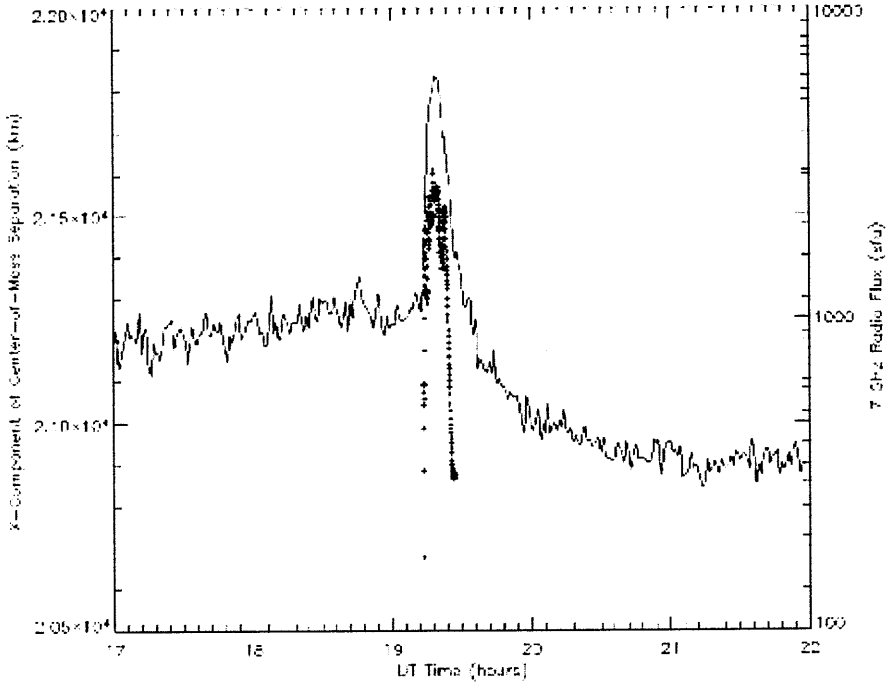

(a)

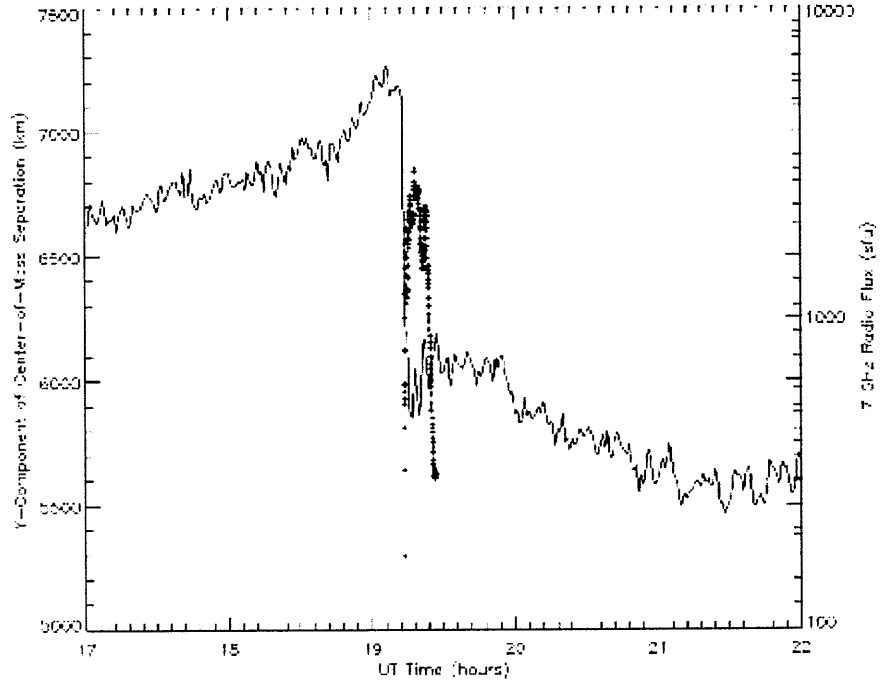

(b)

Figure 4.8 (a) Plot of the X-component of the magnetic flux center-of-mass separation versus time. (b) Plot of the Y-component of the magnetic flux center-of-mass separation versus time. The solid lines indicate the magnetic flux center-of-mass separations. The crosses indicate the 7 GHz radio flux.

CHAPTER 5

RESULTS

5.1 Average Gradient Intensity in the Neutral Line Region

The plot of the average gradient intensity in the neutral line region versus time shows that the average gradient intensity in the neutral line region experienced a permanent increase after the 2001 April 6 solar flare. Since the method used to align the original magnetograms aligned the magnetograms at the pixel level, subpixel discrepancies in the alignment produced small fluctuations in the plot of the average gradient intensity. Smoothing the magnetograms prior to taking the gradient reduced these fluctuations, but did not eliminate them entirely.

In order to calculate the difference between the average gradient intensity in the neutral line region before and after the flare, the mean of the average gradient intensities from 17:42:02 UT to 18:42:02 UT was taken as being representative of the mean average gradient intensity before the flare and the mean of the average gradient intensities from 20:54:02 UT to 21:54:02 UT was taken as being representative of the mean average gradient intensity after the flare. The mean average gradient intensity before the flare was found to be 0.09319 G/km with a standard deviation of 3.220×10^{-4} G/km. The mean average gradient intensity after the flare was found to be 0.09527 G/km with a standard deviation of 2.755×10^{-4} G/km. Thus, the mean difference between the average gradient intensity before and after the flare is 0.00208 G/km. See Figure 5.1.

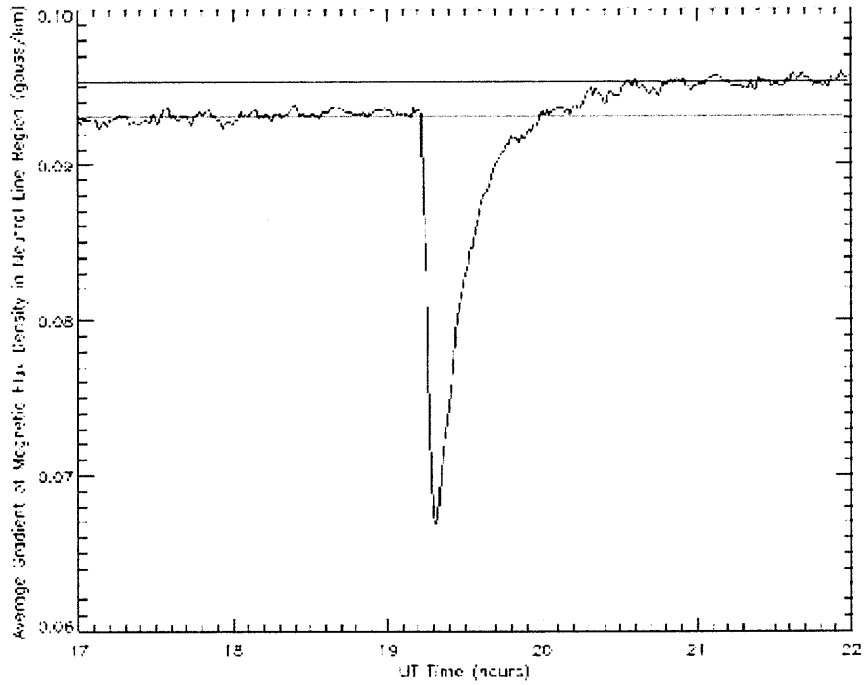

(a)

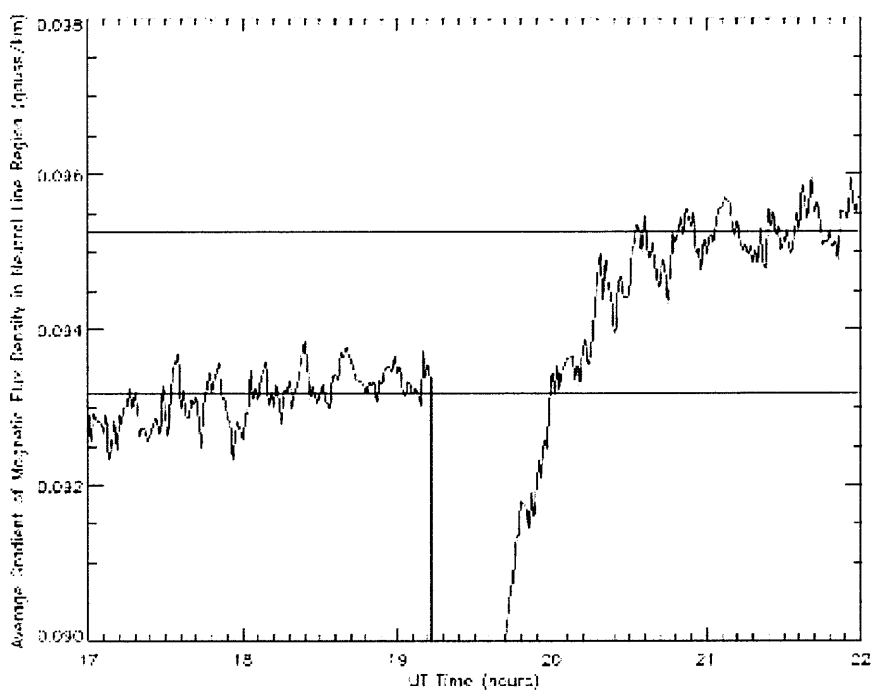

(b)

Figure 5.1 Plot of the average gradient intensity in the neutral line region versus time with the mean average gradient intensities before and after the flare indicated with a range of (a) 0.06 to 0.10 G/km and (b) 0.090 to 0.098 G/km.

To prove that this difference is statistically significant, it is necessary to show that the mean difference divided by the average of the standard deviations is greater than or equal to three. The average standard deviation was determined to be 2.988×10^{-4} G/km. Therefore, the mean difference divided by the average of the standard deviations is 6.96. Since this value is greater than 3 sigma, the mean difference between the average gradient intensity before and after the flare is statistically significant.

5.2 Magnetic Flux Center-of-Mass Separation

Since both the X- and the Y-components of the magnetic flux center-of-mass separation are always positive during the five hour period examined, the positive magnetic flux center-of-mass is located North-West of the negative magnetic flux center-of-mass.

Since only the periods before and after the flare are being considered in this study, the sudden spike in the X-component of the center-of-mass separation plot, which coincides with the flare induced spike in the radio data, can be disregarded. However, the abrupt reduction in the Y-component of the center-of-mass separation, which also coincides with the flare induced spike in the radio data, cannot entirely be ignored since it leads to a permanent reduction in the Y-component of the magnetic flux center-of-mass separation.

The X-component of the center-of-mass separation versus time plot shows that the magnetic flux centers-of-mass separate slightly before the flare and converge towards the neutral line immediately following the flare. The slight separation before the flare is believed to be a consequence of the effects of solar rotation not having been taken into account. The Y-component of the center-of-mass separation versus time plot shows that

the magnetic flux centers-of-mass become increasingly sheared along the neutral line prior to the flare and that this process is suddenly reversed following the flare.

The POLY_FIT function in IDL was used to find the slope of each graph during two hour-long intervals. For the X-component of the center-of-mass separation, the speed of separation determined from the graph is 39 km/hr in the 18:00:02 UT to 19:00:02 UT time interval. The speed of convergence determined from the graph is 89 km/hr in the 20:00:02 UT to 21:00:02 UT time interval. For the Y-component of the center-of-mass separation, the speed of separation determined from the graph is 297 km/hr in the 18:00:02 UT to 19:00:02 UT time interval. The speed of convergence determined from the graph is 265 km/hr in the 20:00:02 UT to 21:00:02 UT time interval. See Figures 5.2 and 5.3. The speeds calculated from the graphs give a rough idea of the actual magnetic flux center-of-mass separation speeds, but not the exact speeds because the effects of solar rotation have not been taken into account.

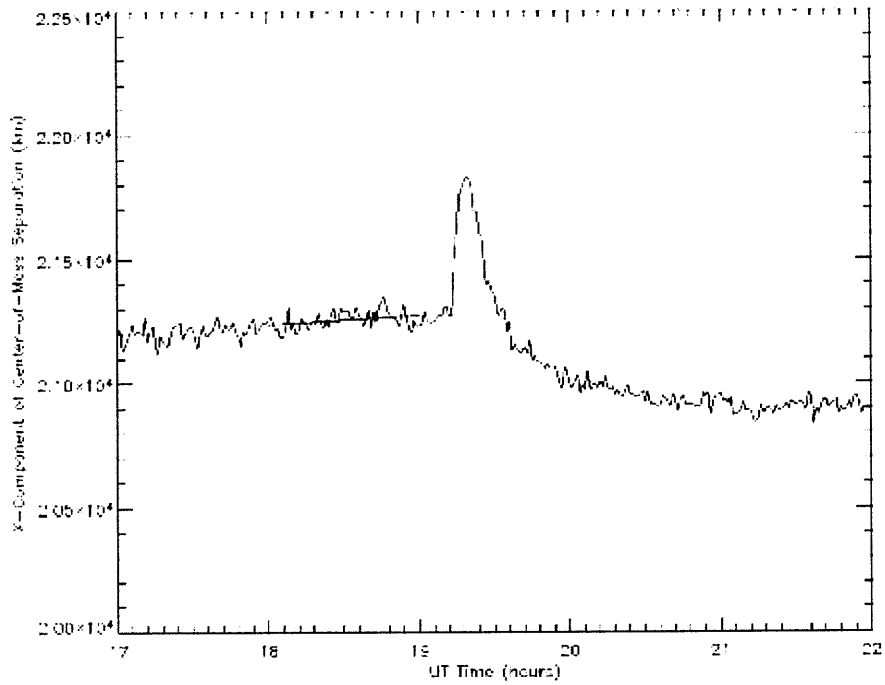

(a)

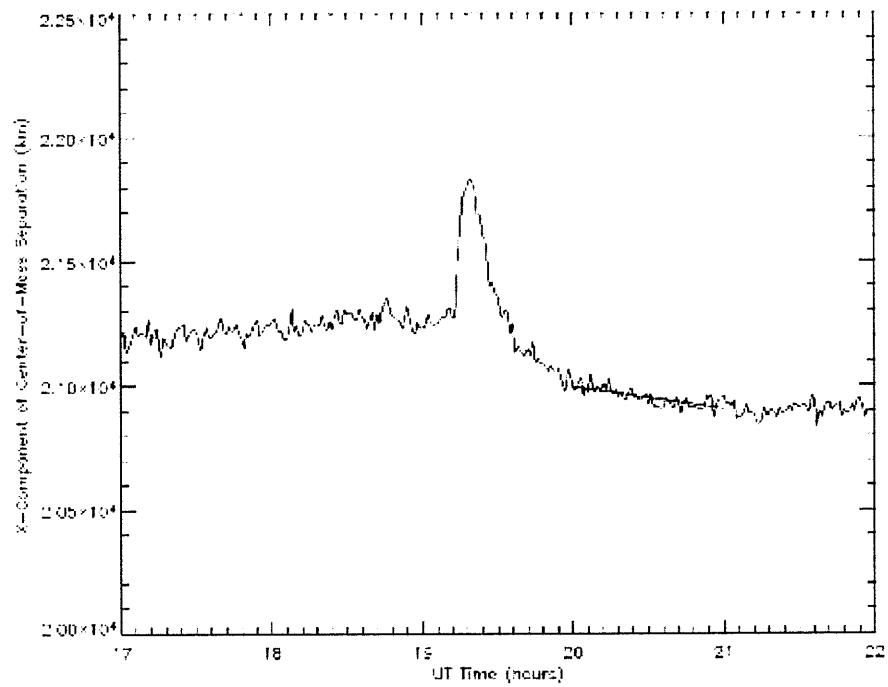

(b)

Figure 5.2 Plot of the X-component of the magnetic flux center-of-mass separation versus time with a trend line for (a) 18:00:02 UT to 19:00:02 UT and (b) 20:00:02 UT to 21:00:02 UT.

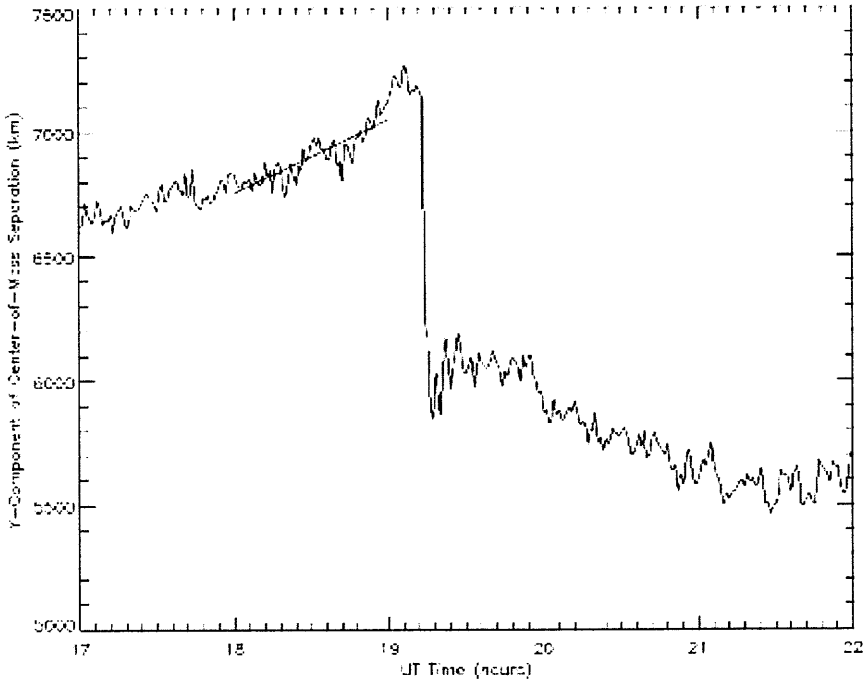

(a)

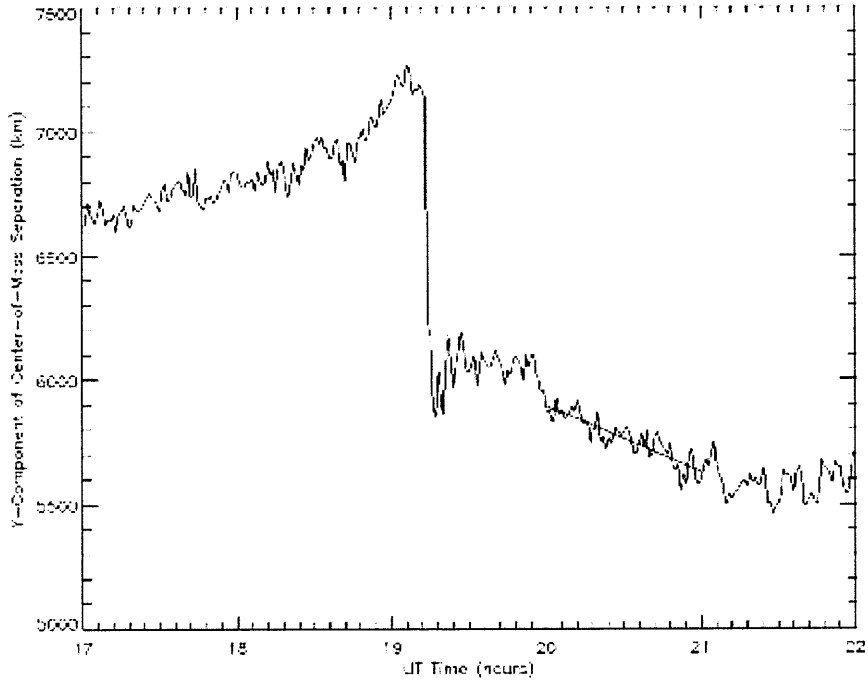

(b)

Figure 5.3 Plot of the Y-component of the magnetic flux center-of-mass separation versus time with a trend line for (a) 18:00:02 UT to 19:00:02 UT and (b) 20:00:02 UT to 21:00:02 UT.

CHAPTER 6

DISCUSSION OF RESULTS

There are two possible reasons for the observed 0.00208 G/km increase in the average gradient intensity in the neutral line region. The first possibility is that new flux emerged along the neutral line during the flare. This could have caused an increase in the average gradient intensity in the neutral line region by increasing the magnetic flux along the neutral line while leaving the magnetic flux along the periphery relatively unchanged. The second possibility is that existing magnetic flux converged towards the neutral line during the flare. This could have caused the increase in the average gradient intensity by increasing the magnetic flux along the neutral line while reducing the magnetic flux along the periphery.

A possible reason for the sudden shift from separation to convergence for the Y-component of the magnetic flux centers-of-mass is that an earthquake-like movement of plasma occurred during the flare and the magnetic field lines were moved along with the plasma.

Wang et al. (2005) applied the same center-of-mass method applied in this project to study the X5.7 flare on 2000 July 14 in AR 9077 (the Bastille Day flare). No variation in the Y-component of the magnetic flux center-of-mass separation was detected. However, a rapid decrease in the X-component of the magnetic flux center-of-mass separation was detected immediately after the flare. The speed of this convergence was calculated to be 216 km/hr for the first hour and a half after the flare and about 108 km/hr afterwards. The speed of convergence of the X-component of the magnetic flux centers-of-mass for the hour long period starting approximately half an hour after the 2001 April

6 flare, 89 km/hr, is relatively close to the speed of convergence of the Bastille Day flare after the first hour and a half. Wang et al. did not find any change in the average gradient of the magnetic flux density in the neutral line region of the Bastille Day flare.

Dr. Haimin Wang applied the same methods used in this project to study the 2001 April 9 flare in AR 9415. See Figure 6.1. A notable postflare increase in the average gradient of the magnetic flux density in the neutral line region was also discovered for the 2001 April 9 flare. The X-component of the magnetic flux center-of-mass separation also decreased after the 2001 April 9 flare indicating a convergence towards the neutral line. Although the Y-component of the magnetic flux center-of-mass separation did not increase prior to the 2001 April 9 flare as it did prior to the 2001 April 6 flare, it did decrease after the flare as it did after the 2001 April 6 flare. However, the decrease in the Y-component of the separation did not occur as suddenly for the 2001 April 9 flare.

The findings of this study support the simple 2-D quadrupolar reconnection model proposed by Liu et al. (2005). The X5.6 solar flare on 2001 April 6 occurred in a δ sunspot. The increase in the average gradient of the magnetic flux in the neutral line region can be explained as the result of magnetic flux convergence towards the neutral line, which triggered magnetic reconnection over the neutral line. In addition, the negative slopes of the X-component of the magnetic flux center-of-mass separation and the Y-component of the magnetic flux center-of-mass separation versus UT time plots subsequent to the flare also support the converging magnetic flux explanation.

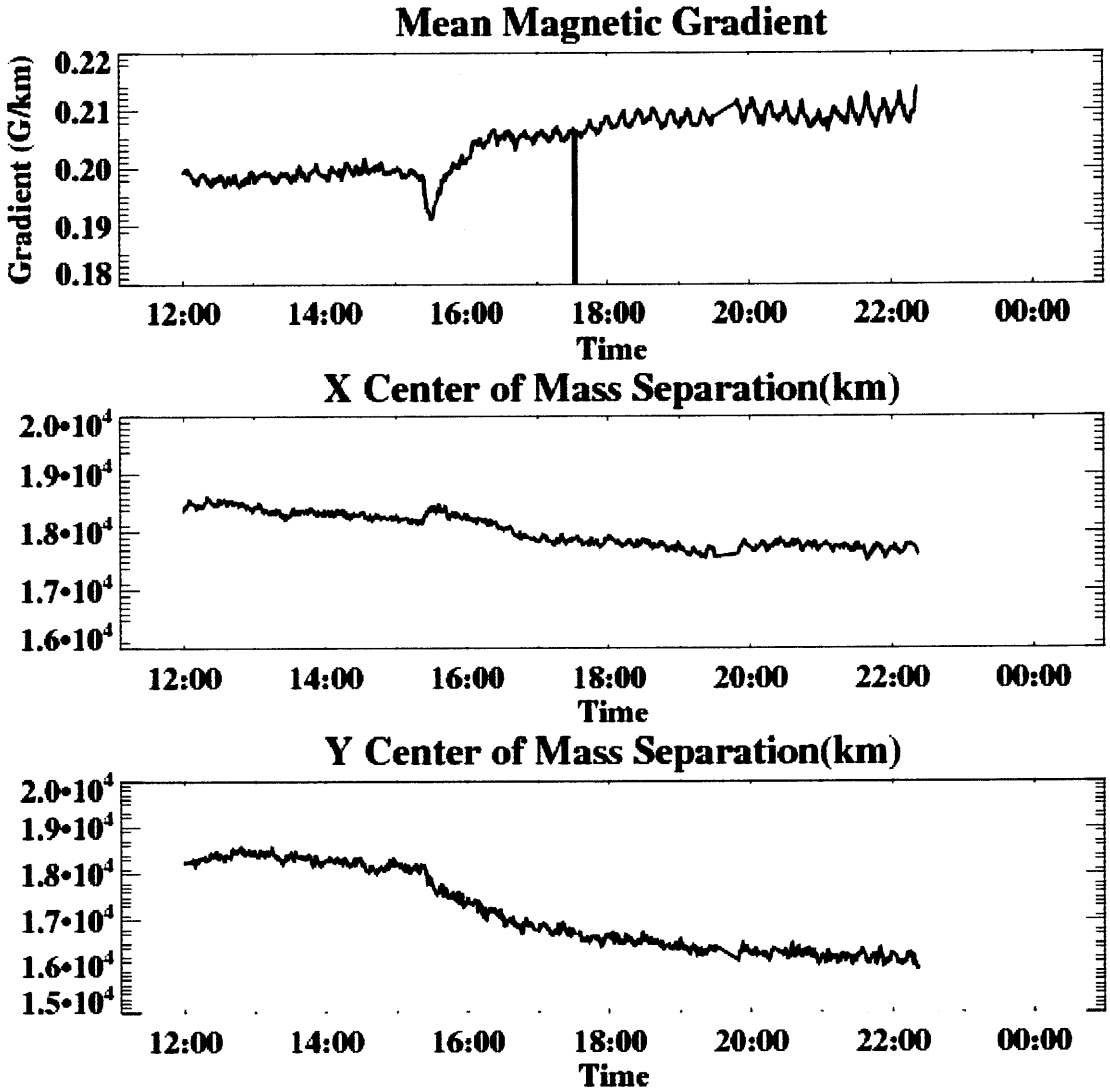

Figure 6.1 Results from an analysis of the solar flare on 2001 April 9 in AR 9415.
Source: Dr. Haimin Wang

Although some of the findings of this study may seem contradictory at first, proper interpretation of the results can resolve the apparent paradox. If the magnetic gradient is proportional to the magnetic shear as Wang et al. (2005) claim, the increase in the average gradient of the magnetic flux around the neutral line implies that the magnetic shear around the neutral line increased following the 2001 April 6 flare. However, the magnetic flux centers-of-mass converged along the neutral line after the flare, which seems to indicate an overall decrease in the magnetic shear of the active

region. This apparent magnetic shear paradox can be resolved by clearly distinguishing between the neutral line region in Figure 4.3 and the whole active region in Figure 4.6. In other words, in spite of an overall decrease in the magnetic shear on the large scale, the magnetic shear apparently increased in local areas, such as the neutral line region, following the flare.

REFERENCES

1. Amari, T., Luciani, J.F., Mikic, Z., & Linker, J. (2000). A twisted flux rope model for coronal mass ejections and two-ribbon flares. Astrophysical Journal, 529, L49-L52.

2. Antiochos, S.K., DeVore, C.R., & Klimchuk, J.A. (1999). A model for solar coronal mass ejections. Astrophysical Journal, 510, 485-493.

3. Antiochos, S.K. (1998). The magnetic topology of solar eruptions. Astrophysical Journal, 502, L181-L184.

4. Chen, J., Wang, H., Zirin, H., & Ai, G. (1994). Solar Physics, 154, 261.

5. Darling, D. (2005). The Encyclopedia of Astrobiology, Astronomy, and Spaceflight: An Alphabetical Guide to the Living Universe [Posted on Web site The Encyclopedia of Astrobiology, Astronomy, and Spaceflight]. Retrieved June 25, 2005 from the World Wide Web: http://www.daviddarling.info/encyclopedia/ETEmain.html.

6. Deng, N., Liu, C., Yang, G., Wang, H., & Denker, C. (2005). Rapid penumbral decay associated with an X2.3 flare in NOAA active region 9026. Astrophysical Journal, 623, 1195-1201.

7. Falconer, D.A., Moore, R.L., & Gary, G.A. (2003). A measure from line-of-sight magnetograms for prediction of coronal mass ejections. Journal of Geophysical Research, 108(A10), SSH 11-1-SSH 11-7.

8. Falconer, D.A., Moore, R.L., & Gary, G.A. (2002). Correlation of the coronal mass ejection productivity of solar active regions with measures of their global nonpotentiality from vector magnetograms: baseline results. Astrophysical Journal, 569, 1016-1025.

9. Keil, S.L., Balasubramaniam, K.S., Bernasconi, P., Smaldone, L.A., & Cauzzi, G. (1994). Solar active region evolution: Comparing models with observations in ASP Conf. Ser. 68, San Francisco, ASP, 265.

10. Kosovichev, A.G. & Zharkova, V.V. (1999). Variations in photospheric magnetic field associated with flares and CMEs. Solar Physics, 190, 459-466.

11. Liu, C., Deng, N., Liu, Y., Falconer, D., Goode, P.R., Denker, C., & Wang, H. (2005). Rapid change of δ spot structure associated with seven major flares. Astrophysical Journal, 622, 722-736.

12. Nishio, M., Yaji, K., Kosugi, T., Nakajima, H., & Sakurai, T. (1997). Magnetic field configuration in impulsive solar flares inferred from coaligned microwave/X-ray images. Astrophysical Journal, 489, 976-991.

13. Phillips, T. (2005). Flare classes [Document posted on Web site SpaceWeather.com]. Retrieved June 25, 2005 from the World Wide Web: http://www.spaceweather.com/glossary/flareclasses.html.

14. Priest, E.R. & Heyvaerts, J. (1974). Solar Physics, 36, 433.

15. Qiu, J., Lee, J., & Gary, D.E. (2004). Impulsive and gradual nonthermal emissions in an X-class flare. Astrophysical Journal, 603, 335-347.

16. Qiu, J. & Gary, D.E. (2003). Flare-related magnetic anomaly with a sign reversal. Astrophysical Journal, 599, 615-625.

17. Schrijver, C.J. & Zwaan, C. (2000). Solar and Stellar Magnetic Activity. New York: Cambridge University Press, 203-205

18. Spirock, T.J., Yurchychyn, V., & Wang, H. (2002). Rapid changes in the longitudinal magnetic field related to the 2001 April 2 X20 flare. Astrophysical Journal, 572, 1072-1076.

19. Stanford-Lockheed Institute for Space Research (2000). The Michelson Doppler Imager [Document posted on Web site MDI]. Retrieved June 25, 2005 from the World Wide Web: http://soi.stanford.edu/.

20. Svestka, Z. (2003). Solar Activity in Dynamic Sun, New York, Cambridge University Press, 245-249.

21. Wang, H., Song, H., Yurchyshyn, V., Deng, Y., Zhang, H., Falconer, D., & Li, J. (2005). Relationship between magnetic gradient and magnetic shear in five super active regions producing great flares. Astrophysical Journal, in press.

22. Wang, H., Liu, C., & Deng, Y. (2005). Re-evaluation of the magnetic structure and evolution associated with the Bastille Day flare on 2000 July 14. Astrophysical Journal, 627, 1031-1039.

23. Wang, H., Spirock, T.J., Qiu, J., Ji, H., Yurchyshyn, V., Moon, Y., Denker, C., & Goode, P.R. (2002). Rapid changes of magnetic fields associated with six X-class flares. Astrophysical Journal, 576, 497-504.

24. Zirin, H. & Liggett, M.A. (1987). Delta sunspots and great flares. Solar Physics, 113, 267-283.